Effects of Regioregularity of π-Conjugated Polymers Composed of Boron *β*-Diketiminate on Their Stimuli-Responsive Luminescence

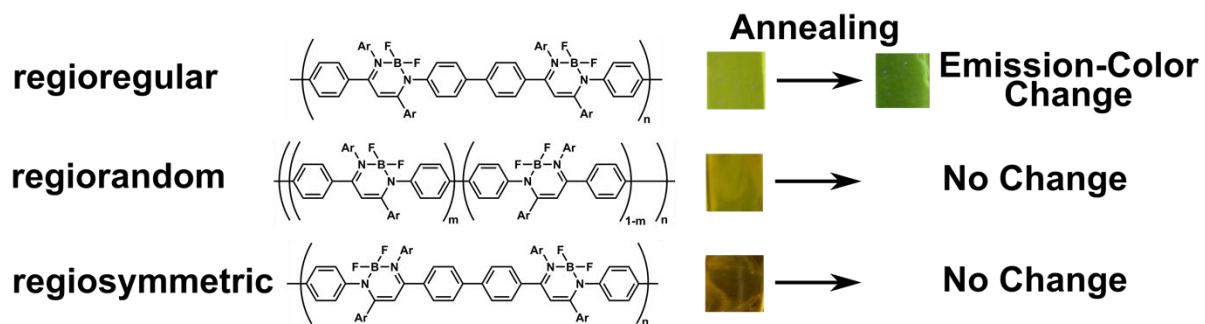*Shunichiro Ito, Misuzu Fukuyama, Kazuo Tanaka,* Yoshiki Chujo*

Department of Polymer Chemistry, Graduate School of Engineering, Kyoto University

Katsura, Nishikyo-ku, Kyoto 615-8510, Japan

E-mail: tanaka@poly.synchem.kyoto-u.ac.jp

TOC Graphic

Abstract

π-Conjugated polymers composed of a boron *β*-diketiminate complex with different regioregularity were synthesized by using Suzuki–Miyaura and Yamamoto couplings. The films formed with the polymers showed luminescence chromism upon exposure to solvent vapors. Most importantly, the chromic behavior depends on the regioregularity of the polymers. Wide-angle X-ray diffraction, thermal analysis, and density functional theory calculations suggest that the chromism could originate from the morphological change in the films and the alternation of the electronic nature of the main chains.

Secondary Abstract

Regioregularity of the luminescent polymers composed of boron β-diketiminate complexes affects their chromic properties. Regioregular, regiorandom, and regiosymmetric polymers were synthesized with AA- and AB-type monomers. Vapochromic luminescence was clearly observed only from the films of the regioregular polymer. It was indicated that the crystallinity in the film states highly depended on the regioregularity. Head-to-head and tail-to-tail linkages in the regiorandom and regiosymmetric polymers might play an important role as an exciton trap.

1. Introduction

π-Conjugated polymers have attracted considerable attention from both academic and industrial researches because of their promising applicability to next-generation optoelectronic devices such as organic light-emitting diodes,[1–3] photovoltaic cells,[4–6] organic field-effect transistors,[7] and chemical and biological sensors.[8] Considering their applications in the solid states, material properties should be governed not only by first-order structures composed of π-conjugated backbones but by higher-order structures involving solid-state morphology. A delicate balance of these two structural components is required to achieve properties desirable for device functions and a sufficiently high solubility for enabling straightforward processing options.[9,10]

The morphological control in the solid states is necessary to improve the optoelectronic device performance not only of conjugated polymers[9,11–14] but also of covalent-organic frameworks.[15] The key factor for morphological control of linear conjugated polymers is the translational symmetry between repeating units or the substructure that comprise several repeating units, along the backbone vector.[16] In addition, the level of organization at single chain level impacts the electronic coupling, secondary structure of the chain, solid-state microstructure, and transport of charge carriers in the solid state. Regioregular poly(3-alkylthiophene) (rr-P3AT), which have head-to-tail (HT) well-mannered linkages, have been widely studied for more than two decades, since the synthesis of rr-P3AT from the corresponding asymmetric Grignard monomers was reported in 1992.[17] Recently, the synthesis of rr-P3AT via the catalyst-transfer polycondensation method controlling the molecular weight and polydispersity was also developed.[18,19] These controlled synthetic methods push forward the development of the study on regioregularity of conjugated polymers. There are many reports on the properties of rr-P3AT

such as higher levels of crystallinity, red-shifted optical absorption,[20,21] higher charge-carrier mobilities,[22] and ordered nanostructures.[23] The presence of other linkages leads to materials that are less prone to crystallization. Furthermore, due to increased steric hindrance, tail-to-tail (TT) linkages decrease the coplanarity of adjacent thiophene heterocycles, and in doing so decrease intrachain electronic coupling. rr-P3AT is more structurally homogeneous so that increases the persistence length, the nucleation density and crystallite size.[24] The many examples of regioregularity controlled conjugated polymers other than rr-P3AT have also been reported.[25,26]

Although the research on regioregularity control focusing on the relationship between morphology and conductivity has been widespread, there are a few reports to offer the relationship between morphology and light-emitting properties.[27,28] One of the problems is in aggregate states of planar conjugated molecules. In aggregate states, there are nonradiative quenching processes due to π–π interactions called aggregation caused quenching (ACQ). One of the solutions to solve this problem is aggregation-induced emission (AIE) properties. Tang *et al.* have reported a series of π-conjugated molecules that were not emissive in solution but significantly emissive in aggregates.[29–32] It was also reported that the alternating copolymers composed of group 13 elements *β*-diketiminate complexes show AIE properties as with the case of boron *β*-diketiminate monomers.[33–36] The polymerization was carried out using typical conjugated comonomers such as fluorene and bithiophene. However, most of these copolymers were regiorandom because asymmetric AA- and BB-type monomers were used for their polymerization.

Herein, we developed the synthesis of boron *β*-diketiminate homopolymers with different regioregularity by employing AB-type monomers. They showed different optical properties and

vapochromism in thin film state because they have different morphology reflecting the single chain regioregularity. Plausible models for the structure–property relationships obtained from the series of analyses are described in this manuscript.

2. Results and Discussion

2.1 Synthesis of Monomers and Homopolymers

Three kinds of boron *β*-diketiminate monomers, boronic pinacol ester and monobromo substituted one (**Bpin-M-Br**) and diiodo substituted ones (**I-M-I** and **I-N-I**), were synthesized following the modified synthetic scheme of the previous works[34–37] as shown in Scheme 1. **I-N-I** was designed for providing a regiosymmetric[38,39] (tail-to-tail-head-to-head, TT-HH) polymer via the homocoupling reaction. The octyl chains were introduced for improving solubility and controlling the conformations and aggregation structures. The chemical structures of **Bpin-M-Br**, **I-M-I** and **I-N-I** were confirmed by ^{1}H, ^{13}C, and ^{11}B NMR spectroscopy and high-resolution mass spectrometry (HRMS).

Polymerization was carried out following the modified synthetic scheme of the previous works[34–36] as shown in Scheme 2. The regioregular boron *β*-diketiminate homopolymer (***rr*-BDP**) was obtained from **Bpin-M-Br** as an AB-type monomer with the palladium-catalyzed Suzuki−Miyaura cross coupling reaction. The regiorandom and regiosymmetric boron *β*-diketiminate homopolymers (***rra*-BDP** and ***rs*-BDP**) were polymerized with **I-M-I** and **I-N-I** as AA-type monomers with the nickel-mediated Yamamoto coupling reaction, respectively. Addition of small amount (0.03 eq.) of **I-M-H** and **H-M-I** allowed us to control molecular weight for ***rra*-BDP** and ***rs*-BDP**, respectively (see experimental section for details). The number-average molecular weight (M_n), weight-average molecular weights (M_w), the molecular weight distribution (M_w/M_n) and the degree of polymerization (*n*) were estimated by size-exclusion chromatography (SEC) in chloroform as an eluent with polystyrene standards (Table 1). Their chemical structures were confirmed by comparing the ^{1}H and ^{11}B NMR spectra of the products to each monomer. Importantly, the signals from the methine protons were observed as

two or three distinct peaks (Figure 1). Considering the specific sequences in **rr-** and **rs-BDP**, we assigned the methine peaks at 5.65, 5.635, and 5.63–5.62 ppm as HT, TT-HH, and terminal moieties, respectively. Integration ratios of each peak were estimated by peak deconvolution with the Lorentzian functions. The repeating unit numbers (n) estimated from these integration ratios were comparable to those from the SEC analysis (Table 1). In addition, it was revealed that **rra-BDP** possesses a slightly HT-rich sequence. On the other hand, the signal-to-noise ratio of $^{13}C\{^{1}H\}$ NMR spectra of these polymers was too low for peak assignment even if the signals from nearly saturated solutions in $CDCl_3$ were accumulated over 24 hours. Nevertheless, all polymers showed good solubility in common organic solvents such as chloroform and dichloromethane, enabling us to fabricate thin films on substrates.

Scheme 1. Synthetic schemes of (a) **Bpin-M-Br** and **I-M-I** and (b) **I-N-I**
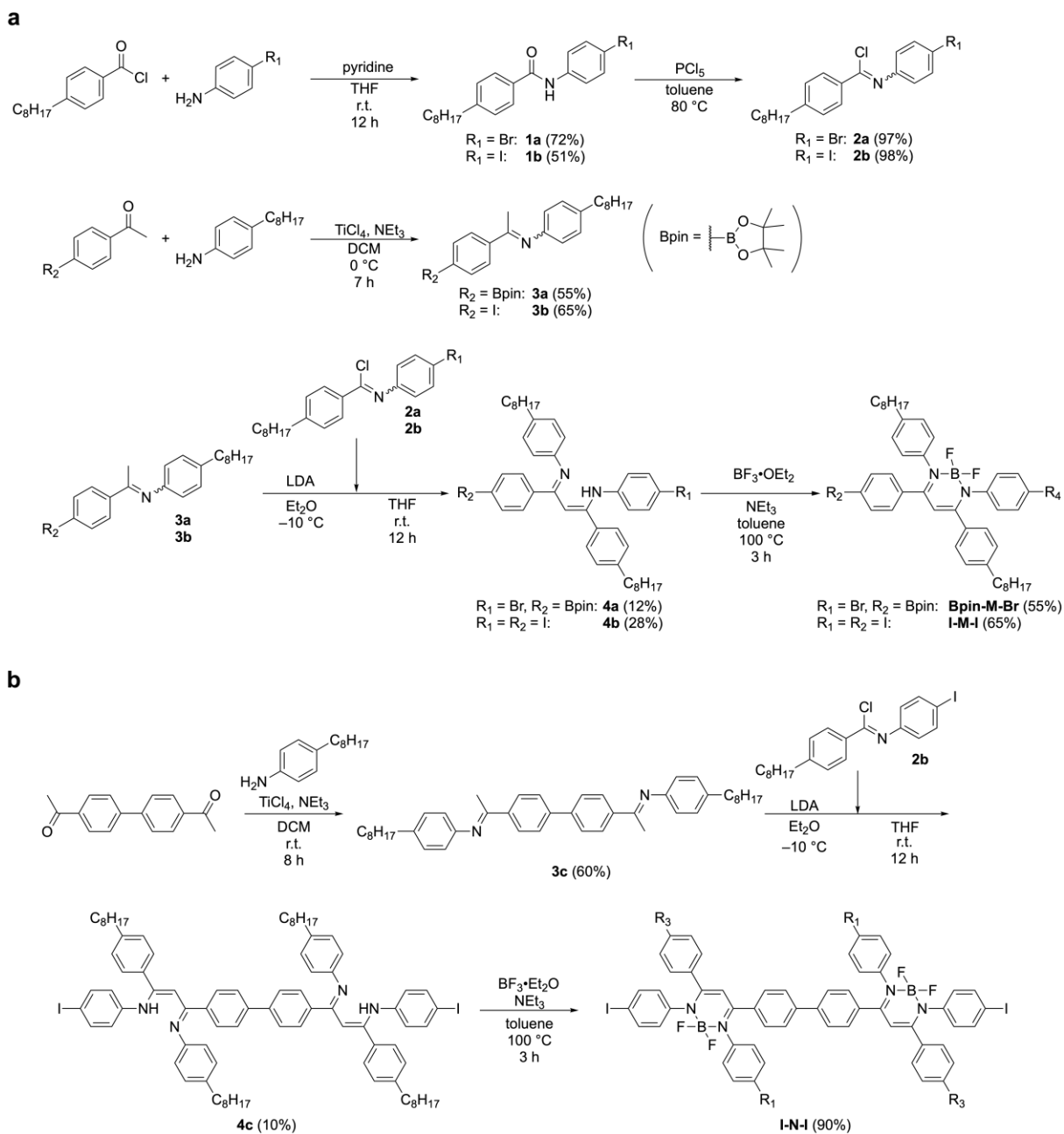
Scheme 2. Synthetic scheme of homopolymers containing boron *β*-diketiminate with different regioregularity
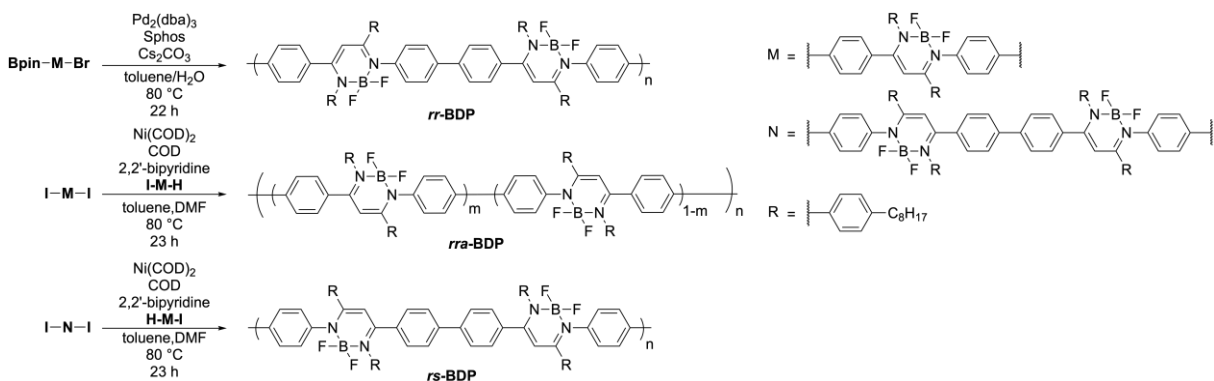
Table 1. Results of polymerization[a]

	Yield	$M_{n, GPC}$	$M_{w, GPC}$	M_w/M_n	n^b
rr-BDP	84%	9,600	21,100	2.2	8 (13)
rra-BDP	83%	10,400	27,400	2.6	8 (11)
rs-BDP	84%	10,900	28,300	2.6	9 (12)

[a] Estimated by SEC with the polystyrene standards in CHCl3. [b] Average number of repeating units calculated from M_n and molecular weights of the repeating units. Estimated values of n from ^{1}H NMR spectra were also shown in the parentheses.
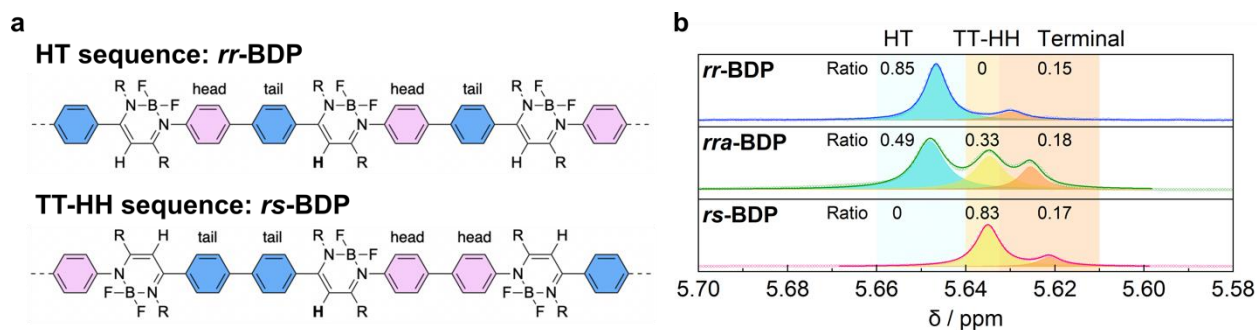

Figure 1. (a) Chemical structures of the head-to-tail (HT) and tail-to-tail-head-to-head (TT-HH) sequences. (b) ^{1}H NMR spectra of the polymers in the region of methine protons: Circles, measured data; shaded, deconvoluted peaks; solid lines, cumulative curves. Integration ratios were shown.

2.2 Photophysical Properties for Dilute Solutions

To evaluate the electronic properties of each polymer without the effect of intermolecular interaction, we measured UV−vis absorption and fluorescence spectra of chloroform solutions (1.0×10^{-5} M based on the number of moles of a complex unit) as shown in Figure 2 and Table 2. In the absorption spectra, all polymers showed absorption bands in almost the same wavelength region, while the onset values were slightly varied (453 nm for **rr-BDP**, 459 nm for **rra-BDP**, and 460 nm for **rs-BDP**). Considered the first-order structures of the polymers, it was suggested the TT-HH linkages (Figure 1a) were the key factor of the bathochromic shifts of the onset value or smaller optical bandgap of **rra-** and **rs-BDP**. It should be mentioned that the absolute photoluminescent quantum yields (Φ) of these solutions were lower than the detection limit (0.01). These significantly low quantum yields should be derived from the fast non-radiative quenching processes involved in the β-diketiminate moiety.[33,40–43]
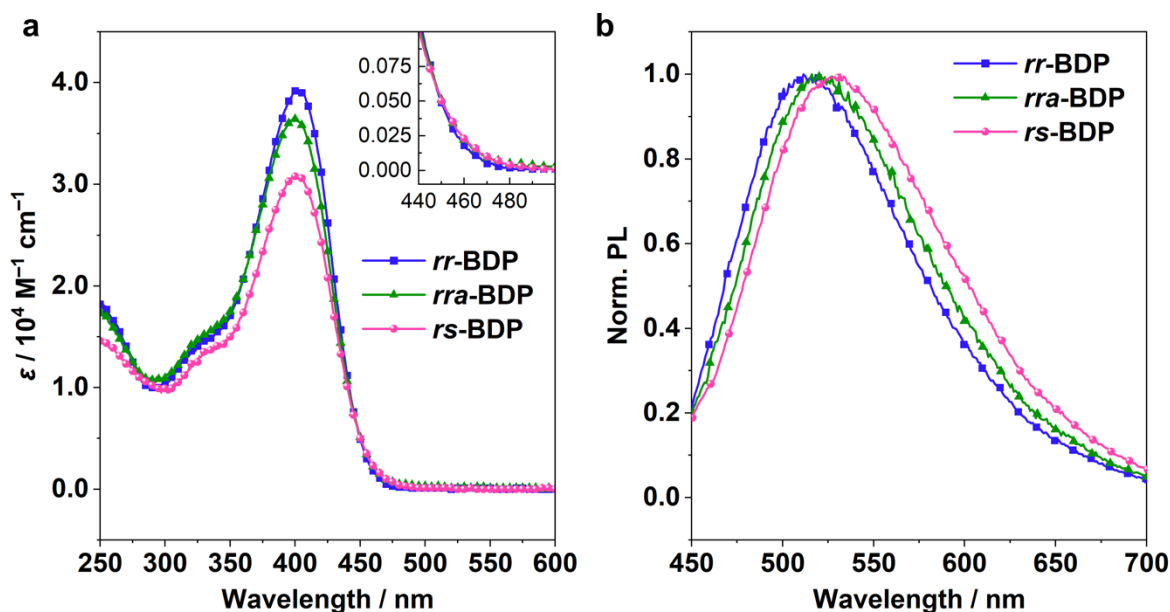
Figure 2. (a) UV–vis absorption and (b) normalized photoluminescence spectra of the synthesized polymers in $CHCl_3$ (1.0×10^{-5} M, PL: excited at each absorption maximum). The inset of absorption spectra shows their region of absorption edge.

Table 2. Photophysical properties of the synthesized polymers in the dilute solutions

	λ_{abs} / nm	ε / $10^5\,M^{-1}\,cm^{-1}$ [a]	λ_{PL} / nm [b]	Φ [c]
rr-BDP	403	0.39	512	<0.01
rra-BDP	402	0.33	519	<0.01
rs-BDP	400	0.31	527	<0.01

[a] Molar absorption coefficient at the absorption maxima. [b] Excited at λ_{abs}. [c] Determined with the integrated sphere method.

2.3 Optical Properties and Vapochromism of Films

The optical properties of the synthesized polymers in film states were evaluated for spin-coated thin films (Figure 3 and Table 3). The films were dried *in vacuo* at ambient temperature for 10 h before photophysical measurements. The maximum absorption wavelengths (403 to 405 nm) were almost the same among the three polymers. In addition, the similar shapes were obtained from the absorption spectra in dilute solutions. This result indicates that intermolecular interaction should be relatively small in the ground state even in the condensed state probably because of the hindered aromatic and aliphatic groups. On the other hand, photoluminescence spectra were different among those polymers (*rr*-BDP, 533 nm; *rra*-BDP, 540 nm; *rs*-BDP, 549 nm). The cause of such bathochromic shifts of *rs*-BDP could be originated from the TT-HH linkages, which are absent in *rr*-BDP and may act as a low-energy exciton trap. This point is

evaluated in detail with quantum chemical calculations, *vide infra*. **rs-BDP** should have higher probability that the excitons generated on polymer chains reach the trap than **rra-BDP** because **rs-BDP** is composed purely on the TT-HH sequence as shown in Figure 1a. Moreover, the photoluminescence quantum yields of these polymers in thin films increased by more than three times compared to those in the dilute solutions. This result means that the synthesized polymers have AIE as well as solid-state emissive properties.
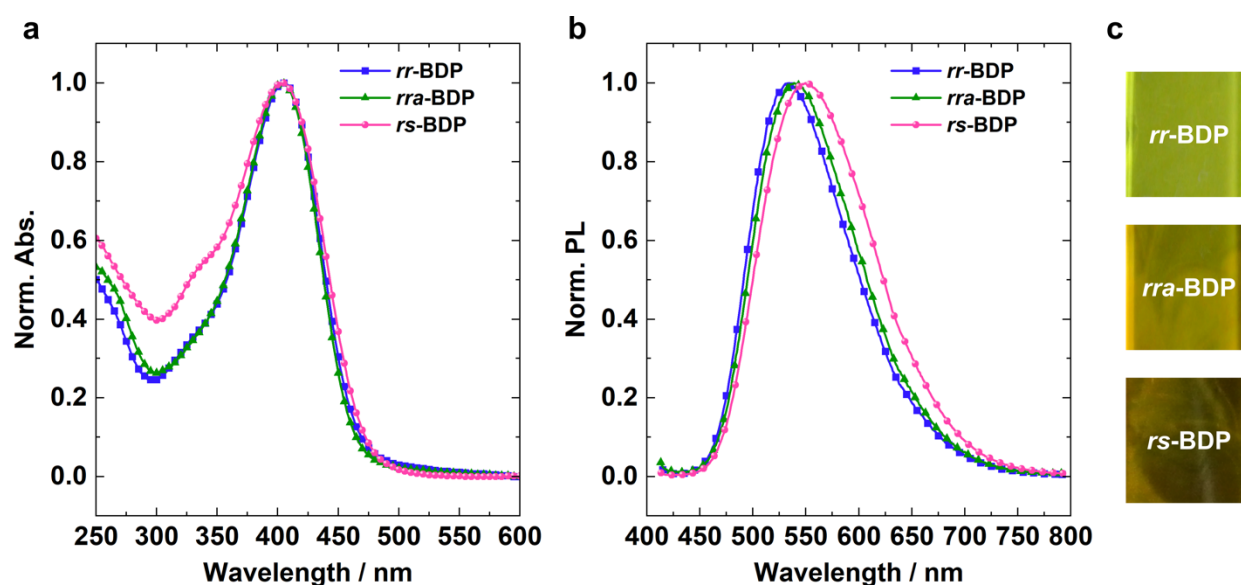

Figure 3. (a) Normalized UV–vis absorption and (b) normalized photoluminescence spectra of the polymers in the spin-coated thin film (PL: excited at each absorption maximum). (c) Photographic images of polymer films under UV (365 nm) irradiation.

Table 3. Photophysical properties of the synthesized polymers in the spin-coated thin-film states

	λ_{abs} / nm	λ_{PL} / nm [a]	Φ [b]
rr-BDP	405	533	0.03
rra-BDP	403	540	0.04
rs-BDP	403	549	0.03

[a] Excited at λ_{abs}. [b] Determined with the integrated sphere method.

2.4 Vapochromism of Films

The spin-coated films responded in luminescent color to solvent vapors. Importantly, the responsivity was dependent on the regioregularity. Solvent-vapor annealing (SVA) is one of the methods to get highly regular structures of polymers predicted at equilibrium.[44] SVA is said to be a more effective annealing process than thermal treatment considering the annealing time and thermal stability of polymers. In SVA, as-casted polymer thin films were exposed to vapors of organic solvents at temperatures typically below the glass transition temperature of polymers to form a swollen and mobile polymer chains on the substrate. On subsequent solvent evaporation, polymer chains can form more well-ordered structures. The as-casted films are kinetically trapped in nonequilibrium and disorganized, in other words, amorphous state, so that SVA process is expected to cause the morphological change from amorphous state to the ordered structure. The annealing process in details is depicted in Experimental Section.

In this experiment, THF, toluene, chloroform, dichloromethane, methanol, hexane, and cyclohexane were used. The good solvents such as THF, toluene, chloroform, and dichloromethane caused significant changes in luminescent color, while the poor solvents (methanol, hexane, and cyclohexane) hardly induced any change. The differences in spectral shifts were slight among the good solvents. UV−vis absorption and photoluminescence spectra of thin films were recorded before and after THF vapor annealing (Figure 4 and Table 4). There is almost no change in absorption spectra of *rr*-BDP, whereas hypsochromic shift was observed in the emission bands from 533 nm to 523 nm. This luminescent color change could be observed by naked eyes (yellowish green to green). The absorption spectra of *rra*-BDP showed a little

bathochromic shift, and that of **rs-BDP** showed by 7 nm bathochromic shift. In addition, there

was no change in the photoluminescence spectra of those two polymers. The shift of the

emission band of **rr-BDP** changed gradually depending on the annealing time (Table S1). The

change in photoluminescence spectra was governed by the behavior of excitons.[45–48] On the

other hand, since the absorption spectra reflect electronic structures in electronically ground

states, the bathochromic shift in absorption spectra of **rra-** and **rs-BDP** suggest that there is
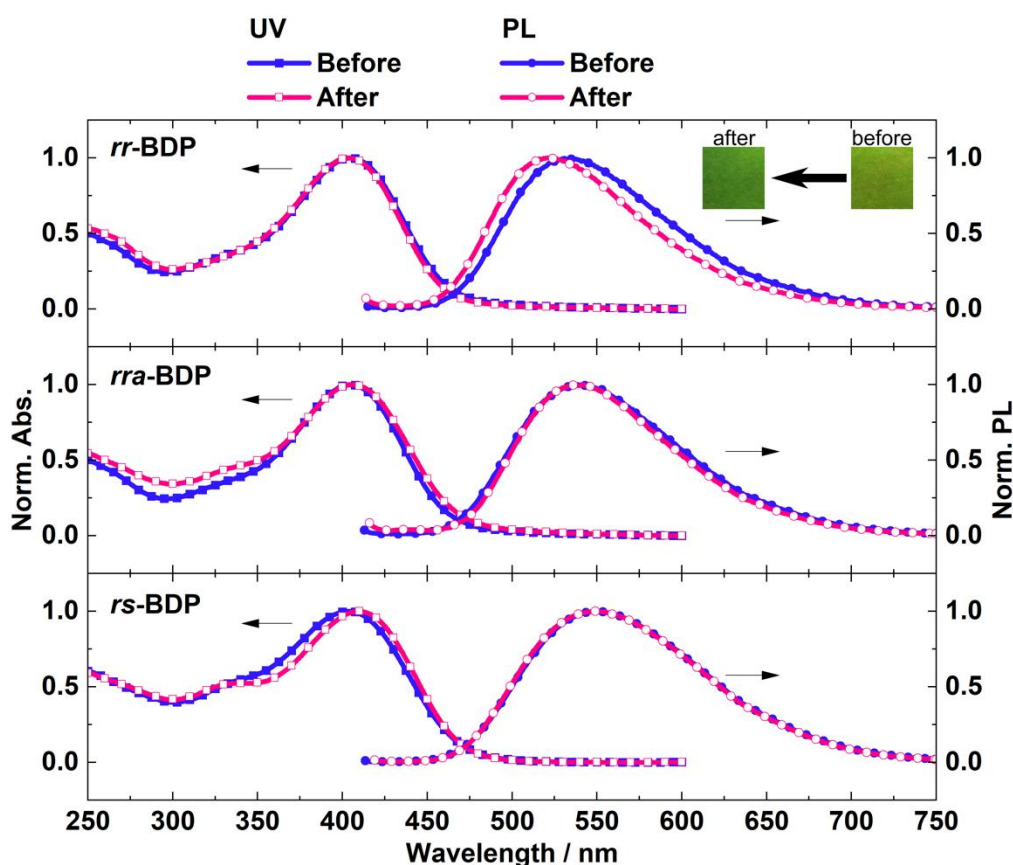
morphological change before and after the SVA.

Figure 4. Normalized UV–vis absorption spectra and normalized photoluminescence spectra of

(top) **rr-BDP**, (middle) **rra-BDP** and (bottom) **rs-BDP** in the spin-coated films before and after

solvent-vapor annealing with THF (PL: excited at each absorption maximum). The inset

represents the photographic images of **rr-BDP** under UV irradiation (365 nm) before and after solvent-vapor annealing.

Table 4. Photophysical properties of the synthesized polymers in the spin-coated thin-film state before and after solvent vapor annealing (SVA)

		λ_{abs}/ nm	λ_{PL} / nm [a]	Φ [b]
rr-BDP	Before SVA	405	533	0.03
	After SVA	404	523	0.04
rra-BDP	Before SVA	403	540	0.04
	After SVA	406	541	0.04
rs-BDP	Before SVA	403	549	0.03
	After SVA	410	549	0.05

[a] Excited at λ_{abs}. [b] Determined with the integrated sphere method.

2.5 Thermal Analysis

   To obtain further insight into the structural change induced by the SVA, we performed differential scanning calorimetry (DSC) (Figure S1 and Table S2). The samples were prepared with the reprecipitation method by pouring a chloroform solution of each polymer into excess amount of methanol. Those powder samples showed the same vapochromism as for the thin films. In the heating curves of **rr-BDP**, the endothermic peaks were observed at 60 and 55 °C before and after SVA, respectively. These transitions could be assigned to the melting points of the aliphatic domains ($T_m^{\text{side chain}}$).[49–51] The corresponding enthalpy of melting (ΔH_m) decreased from 1.68 to 0.29 J/g as the result of the SVA. In addition, the clear glass transition of alkyl sidechains was observed at −61 °C ($T_g^{\text{side chain}}$) only after the SVA, whereas the vague glass transition before the annealing was detected at −56 °C. These results suggest that the aliphatic

domains in the samples of ***rr*-BDP** were mainly composed of amorphous after the SVA. The first and second cooling cycles of ***rr*-BDP** showed only glass transition of alkyl side chain.

The decrease in the ΔH_m caused by the SVA was also observed for ***rra*-BDP** (from 1.55 to 0.44 J/g). In addition, T_g's of the aliphatic groups were also observed before (–61.9 °C) and after (–65.9 °C) the SVA. Furthermore, in ***rra*-BDP**, the glass transition attributed to the aromatic domains was also observed at 143 °C ($T_g^{\text{main chain}}$), and it appeared to be broad endothermic peak after the annealing possibly because of enthalpy relaxation. In other words, the glassy state in the aromatic domains became more stable after the SVA. The second cycle of ***rra*-BDP** showed the T_g of both aliphatic and aromatic domains.

The heating curves for ***rs*-BDP** also showed the endothermic peaks attributed to aliphatic domains both before and after the SVA, meanwhile there was almost no change in the values of ΔH_m (1.26 and 1.11 J/g). Figure S2 shows the DSC measurements under different conditions and samples for ***rs*-BDP**. The effects of heating rate, molecular weight, and thermal annealing (TA) were considered. The $T_m^{\text{side chain}}$ depended hardly on the heating rate, and there is only slight dependence of the T_{endo} on M_n. However, the sample after TA at 70 °C for 2 hours showed T_{endo} at higher temperature (93 °C), and this could be explained by the growth of the crystalline domains composed of the alkyl side chains. These observations suggested that the T_{endo}'s are attributed to the melting points of the aliphatic domains. The T_g of the main chains and enthalpy relaxation were also observed in this case, while the T_g of the side chains was hardly observed. It is suggested that the aliphatic domains of ***rs*-BDP** should possess a relatively ordered structure before and after the SVA compared to the other polymers.

2.6 Wide Angle X-ray Diffraction Analyses

To survey the morphological changes by the SVA, we measured grazing-incident wide-angle X-ray diffraction (GI-WAXD) for films on a quartz substrate (Figure 5 and Table 5). The samples were prepared by the drop-casting method. There were broad diffraction peaks in the profiles of ***rr*-BDP** after vapor annealing. The broadness of these peaks indicates that the domain size of ordered structures in ***rr*-BDP** is small. Although the peak at 4.75 degree was observed only in the out-of-plane measurement, the peaks at 6.9 degree were observed both in the out-of-plane and in-plane measurements. Consequently, there might be weak preferred orientation. These two peaks could be attributed to aliphatic domains where the π-conjugated backbones and the alkyl sidechains were loosely separated.[52,53] These aliphatic nanodomains were observed all synthesized polymers before SVA. This observation corresponds to the results of the DSC analyses where T_g of main and side chains were separately observed.

The out-of-plane profile of ***rs*-BDP** presented the sharpest diffraction peaks among the three synthesized polymers. On the other hand, the in-plane profile showed no such a sharp peak, suggesting preferred orientation. In the out-of-plane measurement, in addition to the first peak at 5.48° (*d*-spacing = 16.8 Å), the second peak at 10.8° (*d*-spacing = 8.4 Å) was detected. This fact strongly suggests that ***rs*-BDP** forms highly ordered structure. Taking the model structure of ***rs*-BDP** into account (Figure 5b), these results propose that ***rs*-BDP** could form a lamella-like structure. This lamella would be composed of interdigitated alkyl sidechains separating π-backbones by 16.8 Å and would exhibit the edge-on orientation (Figure 5c). The weak peaks at 6–7° (*d*-spacing = 12–13 Å) observed both in the out-of- and in-plane profiles could be attributed to the translational (pseudo)symmetry along with the π-conjugated backbones. The domain size of ordered structure in ***rs*-BDP** was estimated to be about 100 Å (grain diameter) by using a fundamental parameter method. Although the diffraction peaks were weak, similar trend was

observed in the profiles of ***rra*-BDP**. Therefore, ***rra*-BDP** partly forms the similar lamella-like

structure. It is implied that the TT-HH linkage, which is absent in ***rr*-BDP**, acts as the important

role in the formation of such ordered structures. It is worth to note that the no apparent peak

assigned to inter-chain packing such as a π–π stacking was observed from all polymers. This is

likely because the bulky aromatic rings restrict such inter-chain interactions. Therefore, the

photophysical properties of these polymers in thin films should be derived from discrete single
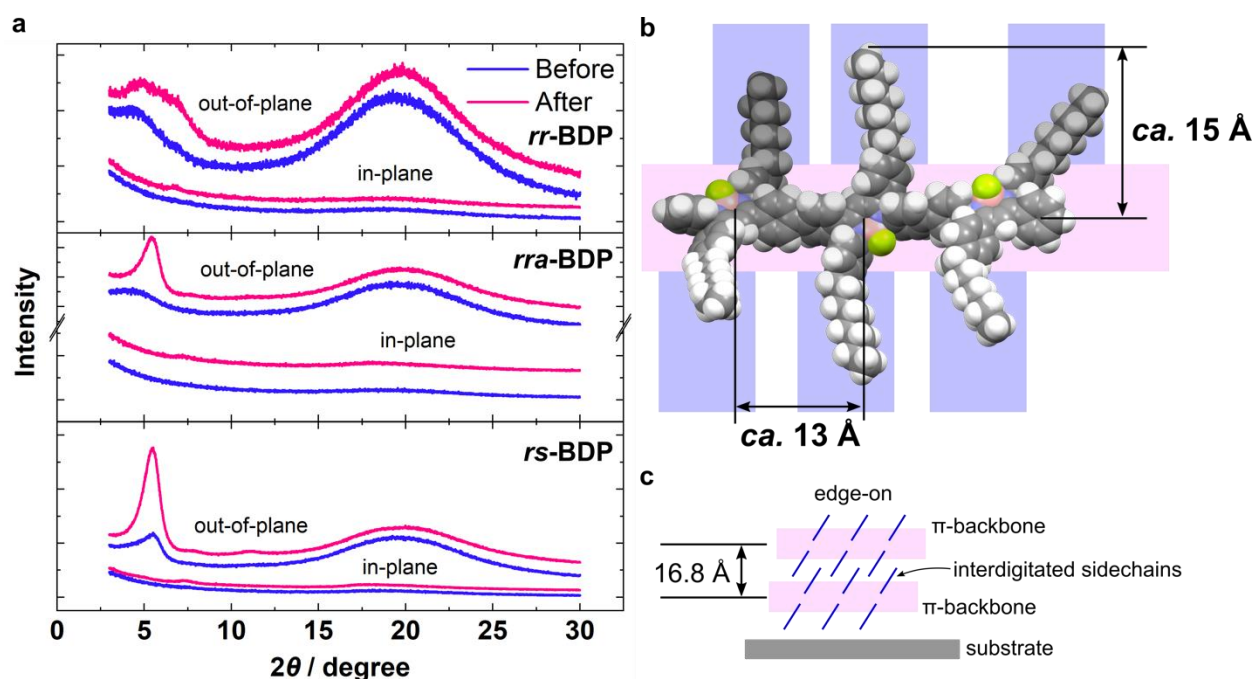
polymer chains.

Figure 5. (a) GI-WAXD patterns of before (blue) and after (magenta) vapor annealing. The

upper parts are out-of-plane and lower parts are in-plane measurements. (b) Optimized model

structure for ***rs*-BDP**. π-Backbone and aliphatic sidechains are highlighted with pink and blue,

respectively. (c) Plausible interdigitate packing structure of ***rra*-BDP** and ***rs*-BDP** in film states.

Table 5. Summary of the diffraction peaks of WAXD analyses after SVA

		Out-of-plane		In-plane
rr-BDP	2θ / degree	4.75	6.96	6.69
	d / Å	18.6	12.3	13.2
rra-BDP	2θ / degree	5.47	6.69	7.10
	d / Å	16.3	13.2	12.5
rs-BDP	2θ / degree	5.48	10.8	7.40
	d / Å	16.1	8.14	11.9

2.7 DFT Calculations for Model Compounds

In order to examine the effects of the difference of linkages, we performed density functional theory (DFT) and time-dependent DFT (TD-DFT) calculations with model structures at the B3LYP level of theory with 6-31G(d) basis set using the Gaussian 16 program package.[54] The models are the trimer for **rr-BDP**, which has two HT linkages (**rr-3**) and that for **rs-BDP**, which has TT-HH linkages (**rr-3**) as shown in Figure 6. Methyl groups were introduced instead of the octyl alkyl chains for simplification. All the optimized structures were confirmed as each local minimum by using frequency calculations at the same level of theory. Figure 6 shows the optimized structures of the trimers. **rr-3** seemed to possess a disarrayed structure probably because of the HT interactions between the dipole moments of the repeating units and the steric repulsion of alkyl sidechains. On the other hand, **rs-3** showed the more arrayed main-chain conformation than **rr-3**, because there is almost no repulsive interaction between the side chains and the local dipoles are enabled to align antiparallel each other so that all the dipoles are canceled out along the whole chain. Such relatively arrayed main-chain conformation of **rs-3** may result in the lamella-like ordered structure in the film state.
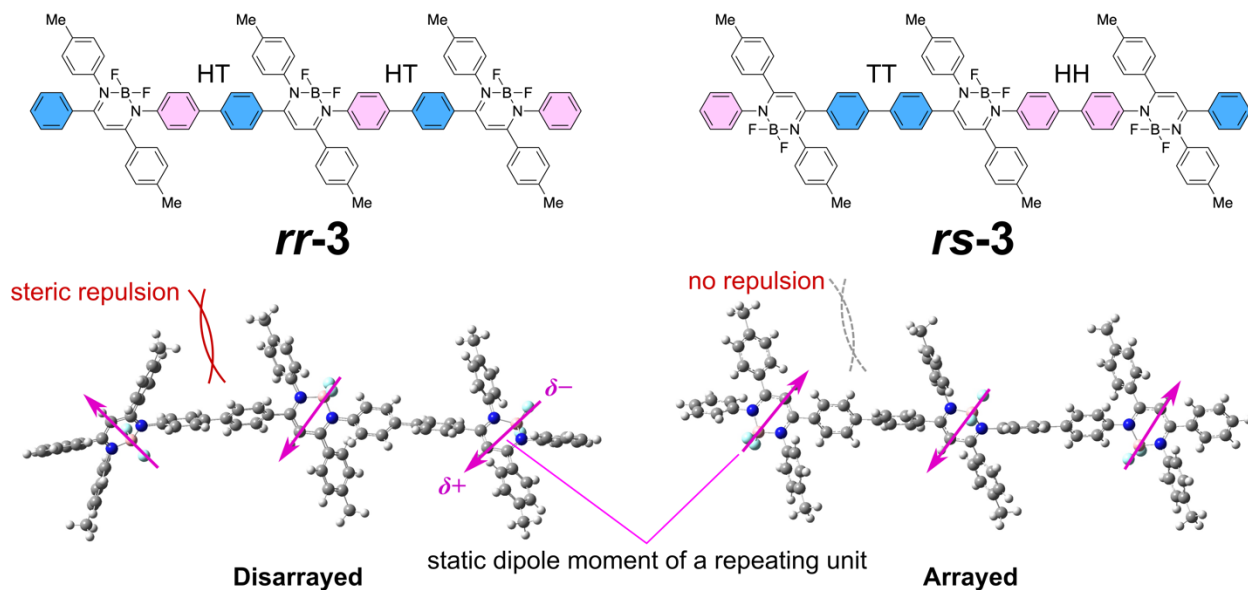
Figure 6. The optimized structures of the model compounds obtained from the DFT calculations. Red curves denote steric repulsion between the side chains. Magenta arrows show the electrostatic dipole moment vectors of the repeating units.

The electronic structures of these trimers were also investigated by DFT and TD-DFT calculations. The calculated Kohn–Sham (KS) frontier molecular orbital distributions and the energy diagrams of *rr*-**3** and *rs*-**3** are shown in Figure 7. Importantly, the highest occupied molecular orbital (HOMO) of *rs*-**3** (–5.38 eV) located at the significantly higher energy region than that of *rr*-**3** (–5.47 eV). This observation suggests that the electronic interaction of HOMOs between the repeating units through the HH connections should be significantly strong compared to the other connections. The lowest unoccupied molecular orbital (LUMO) of *rs*-**3** (–2.02 eV), on the other hand, was mainly located at the TT-connected moiety. These results suggest that *rs*-**3** exhibits intramolecular charge transfer (ICT) character, and this is one of the plausible reasons for the smaller bandgap than *rr*-**3**. The results of TD-DFT calculation indicated that the S_1 state should be composed mainly of the HOMO–LUMO transition (82%) and they also suggest the

ICT characters of *rs*-**3** (Table 7). Indeed, Lippert–Mataga plots of *rra*-**BDP** and *rs*-**BDP**, which possess both HH and TT connections, clearly showed positive slopes indicating the ICT property of the transitions (Figure S3 and Table S3). Overall, the HH-TT sequence should be responsible for the lower-energy ICT-type excited states observed in *rs*- and *rra*-**BDP**, indicating that this linkage should act as a low-energy exciton trap in these polymers.

In contrast, the S_1 electronic state of *rr*-**BDP** showed no ICT property. The HOMO (out-of-phase orbital interaction) and HOMO–1 of *rr*-**3** (in-phase orbital interaction) were degenerated ($\Delta E = 0.02$ eV). This fact indicates that the electronic interaction through the HT-connection is not effective. The LUMO of *rr*-**3** was distributed over the two adjacent units where the main chain was bent due to the steric repulsion. Such repulsive interactions between the side chains should be distributed statistically over the conjugated backbone of the polymer. Additionally, the S_1 state of *rs*-**3** was composed not only of HOMO–LUMO (53%) but also HOMO–1–LUMO (15%) and HOMO–LUMO+1 (15%) (Table 7). These results imply that the transition of *rr*-**BDP** should occur without the specific ICT. The Lippert–Mataga plot showed no positive slope, supporting these results of the calculations (Figure S3 and Table S3). Consequently, *rr*-**BDP** showed the highest-energy emission among the synthesized polymers in both solution and film states.
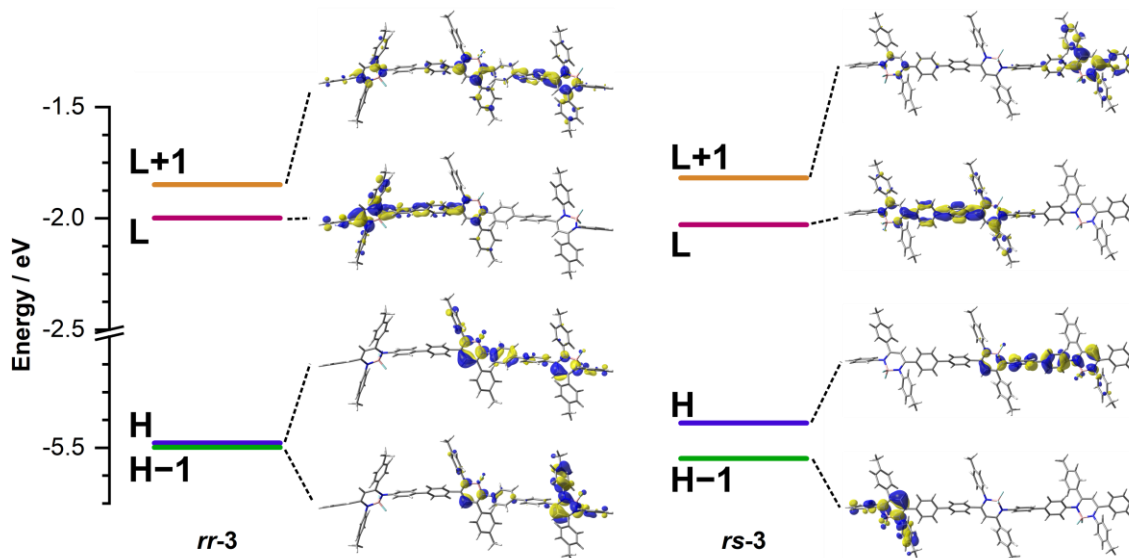
Figure 7. Energy diagrams and Kohn–Sham frontier orbital distributions of the model compounds *rr*-**3** and *rs*-**3** obtained from the DFT calculations. H and L denote HOMO and LUMO, respectively.

Table 7. Calculated parameters of the S_0–S_1 electronic transitions of *rr*-**3** and *rs*-**3**[a]

Compound	E / eV [b]	λ / nm	f [c]	Composition [d]	Coefficient [e]
rr-**3**	3.17	392	1.62	H–2 → L	0.20664
				H–1 → L	0.27243
				H → L	0.51373
				H → L+1	0.27042
rs-**3**	3.03	409	1.03	H → L	0.64092
				H → L+1	-0.22321

[a] Calculated at the (TD-)B3LYP/6-31G(d,p) level of theory. [b] Transition energy. [c] Oscillator strength. [d] H and L denote HOMO and LUMO, respectively. [e] Configuration-interaction expansion coefficient.

2.8 Plausible Mechanism of the Regioregularity-Dependent Vapochromic Fluorescence

A plausible mechanism of the vapochromism is discussed here (Figure 8). As mentioned in the GI-WAXD section, the photophysical properties of these synthesized polymers should be governed by discrete single chains even in the film state because of the weak interchain interactions. Firstly, the changes in the film structures and photophysical properties are considered for **rr-BDP**. In as-cast films, **rr-BDP** showed the amorphous structure according to the DSC (Figure S1) and the GI-WAXD (Figure 4) data. Such amorphous state possesses large free volumes accepting a structural relaxation at electronically excited states. The SVA allows the reorientation of polymer chains. In the annealed films of **rr-BDP**, there were weakly but more ordered structures indicated by the GI-WAXD analysis. Consequently, the structural relaxation at the excited states should be hampered because of the decrease of free volume after the SVA. As a result, the photoluminescence spectra of the annealed samples showed hypsochromic shift compared to those of as-cast films (Figure 4). On the other hand, the **rr-BDP** films are composed mainly of amorphous phase both before and after SVA. Thus, peak shift was hardly observed in its absorption spectra. The DFT calculations suggested that the main chains of **rr-BDP** possess the disarrayed structure due to the HT sequence (Figure 6). Such cluttered main chains should lead to the formation of the amorphous or the weakly ordered film structures.

Secondly, as for **rra-** and **rs-BDPs**, much more ordered structures of their main and side chains were indicated strongly by the GI-WAXD and the DFT calculations. The ordered structures would enhance π-conjugation along the mainchains, leading to the lowering the exciton bands of the polymers. Consequently, the bathochromic shifts were detected in the spectra of **rra-** and **rs-BDP**. As indicated from the DFT calculations, the TT-HH alternative linkages could serve as a low-energy exciton trap of excitons because of its ICT property. The

excitons generated on the polymer chains should be always trapped in this low-energy region, even if the solid-state structures changed by the SVA. In addition, the energy of the trap would not be affected by the SVA because the ICT state is localized at the TT-HH sequence. Consequently, the photoluminescence spectra of **rs-** and **rra-BDP** were hardly changed by the SVA. Such an exciton trap is absent in **rr-BDP** because the TT-HH sequence is not included in the mainchain as shown in the ^{1}H NMR spectrum (Figure 1).
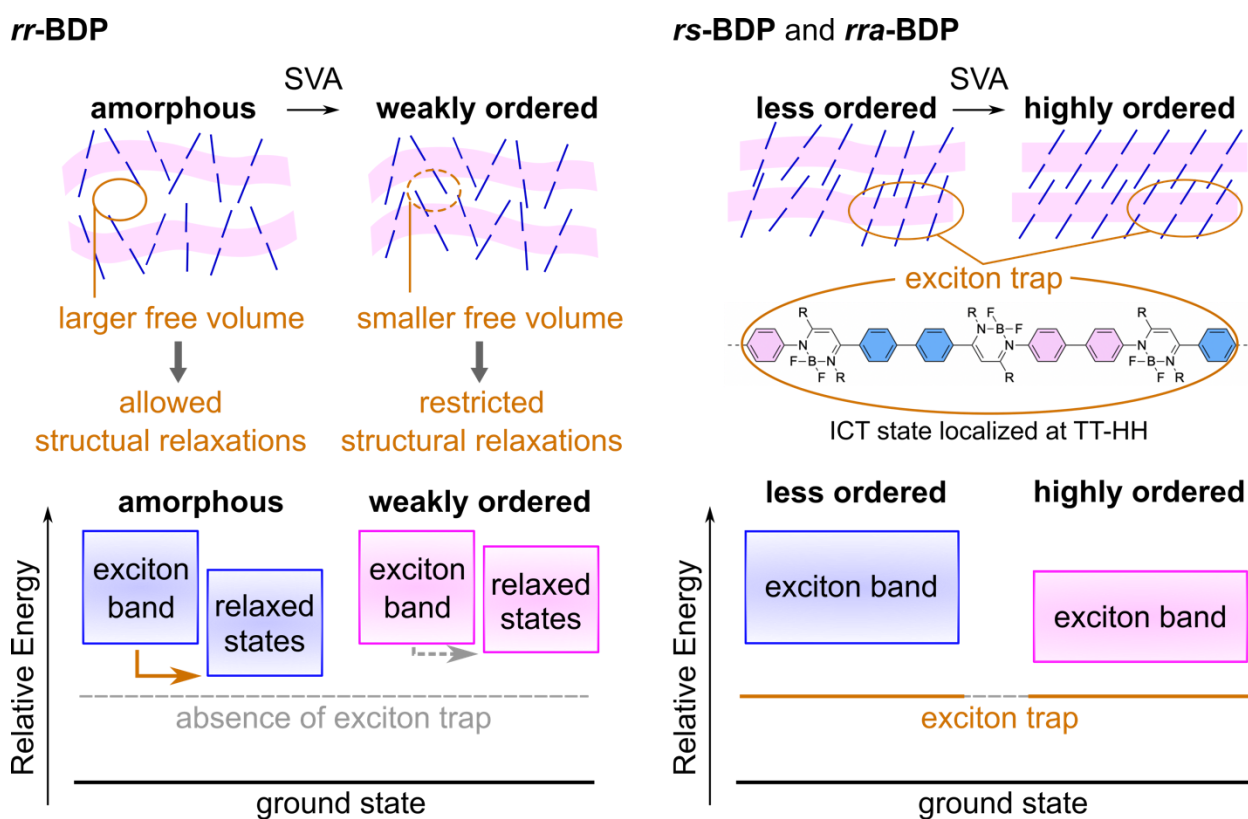
Figure 8. Schematic representation of a plausible mechanisms of the regioregularity-dependent fluorescence of the polymers.

3. Conclusions

Homopolymers composed of boron *β*-diketiminate complexes with different regioregularity were successfully synthesized with the corresponding AA-type and AB-type monomers. Their thin films showed different optical properties and vapochromism depending on their regioregularity. The regioregular polymer showed vapochromic luminescence, whereas the regiorandom and regiosymmetric polymers hardly exhibited such significant changes in their luminescent spectra. The results of DSC and WAXD measurements proposed that the regioregularity of the polymers could affect the sidechain assembly leading to the lamella-like ordered structure. The solvent-vapor annealing allowed the polymers to reorder and enhance the crystallinity and the edge-on orientation, especially for the regiorandom and regiosymmetric polymers. Moreover, the series of DFT calculations suggested that the TT-HH linkages involved in the regiorandom and regiosymmetric polymers could provide a low-energy exciton trap. The excitons on these polymers might be collected in the traps, even if the films were annealed or not. Therefore, these two polymers did not change their emission color. Meanwhile, the annealing process could reduce free volumes in the films for the regioregular polymer, resulting in the restriction of structural relaxations in the excited states. Therefore, the emission color of the regioregular polymer showed hypsochromic shift by the SVA. These results would open a new way to create stimuli-responsive materials based on regioregularity control.

Acknowledgments

Conflict of Interest

The authors declare no conflict of interest.

References

[1] A. C. Grimsdale, K. L. Chan, R. E. Martin, P. G. Jokisz, A. B. Holmes, *Chem. Rev.* **2009**, *109*, 897.

[2] N. Tessler, V. Medvedev, M. Kazes, S. Kan, U. Banin, *Science* **2002**, *295*, 1506.

[3] A. Sandström, H. F. Dam, F. C. Krebs, L. Edman, *Nat. Commun.* **2012**, *3*, 1002.

[4] Y.-J. Cheng, S.-H. Yang, C.-S. Hsu, *Chem. Rev.* **2009**, *109*, 5868.

[5] L. Lu, T. Zheng, Q. Wu, A. M. Schneider, D. Zhao, L. Yu, *Chem. Rev.* **2015**, *115*, 12666.

[6] E. Dauzon, X. Sallenave, C. Plesse, F. Goubard, A. Amassian, T. D. Anthopoulos, *Adv. Mater.* **2021**, *33*, 2101469.

[7] H. Sirringhaus, *Adv. Mater.* **2014**, *26*, 1319.

[8] D. T. McQuade, A. E. Pullen, T. M. Swager, *Chem. Rev.* **2000**, *100*, 2537.

[9] J. Mei, Z. Bao, *Chem. Mater.* **2014**, *26*, 604.

[10] I. Osaka, M. Saito, T. Koganezawa, K. Takimiya, *Adv. Mater.* **2014**, *26*, 331.

[11] J. Li, X. Peng, C. Huang, Q. Qi, W.-Y. Lai, W. Huang, *Polym. Chem.* **2018**, *9*, 5278.

[12] X.-C. Li, Y. Xue, W. Song, Y. Yan, J. Min, F. Liu, X. Liu, W.-Y. Lai, W. Huang, *Research* **2020**, *2020*, 1.

[13] Y. Jiang, K. F. Li, K. Gao, H. Lin, H. L. Tam, Y. Liu, Y. Shu, K. Wong, W. Lai, K. W. Cheah, W. Huang, *Angew. Chem. Int. Ed.* **2021**, *60*, 10007.

[14] F. Zhao, C. Wang, X. Zhan, *Adv. Energy. Mater.* **2018**, *8*, 1703147.

[15] Y.-Y. Liu, X.-C. Li, S. Wang, T. Cheng, H. Yang, C. Liu, Y. Gong, W.-Y. Lai, W. Huang, *Nat. Commun.* **2020**, *11*, 5561.

[16] L. Ying, F. Huang, G. C. Bazan, *Nat. Commun.* **2017**, *8*, 14047.

[17] R. D. McCullough, R. D. Lowe, *Chem. Commun.* **1992**, 70.

[18] T. Yokozawa, Y. Ohta, *Chem. Commun.* **2013**, *49*, 8281.

[19] T. Yokozawa, Y. Ohta, *Chem. Rev.* **2016**, *116*, 1950.

[20] Y. Kim, S. Cook, S. M. Tuladhar, S. A. Choulis, J. Nelson, J. R. Durrant, D. D. C. Bradley, M. Giles, I. McCulloch, C.-S. Ha, M. Ree, *Nat. Mater.* **2006**, *5*, 197.

[21] J. Guo, H. Ohkita, H. Benten, S. Ito, *J. Am. Chem. Soc.* **2009**, *131*, 16869.

[22] H. Sirringhaus, P. J. Brown, R. H. Friend, M. M. Nielsen, K. Bechgaard, B. M. W. Langeveld-Voss, A. J. H. Spiering, R. A. J. Janssen, E. W. Meijer, P. Herwig, D. M. de Leeuw, *Nature* **1999**, *401*, 685.

[23] J. Liu, M. Arif, J. Zou, S. I. Khondaker, L. Zhai, *Macromolecules* **2009**, *42*, 9390.

[24] R. J. Kline, M. D. McGehee, E. N. Kadnikova, J. Liu, J. M. J. Fréchet, M. F. Toney, *Macromolecules* **2005**, *38*, 3312.

[25] L. Ying, B. B. Y. Hsu, H. Zhan, G. C. Welch, P. Zalar, L. A. Perez, E. J. Kramer, T.-Q. Nguyen, A. J. Heeger, W.-Y. Wong, G. C. Bazan, *J. Am. Chem. Soc.* **2011**, *133*, 18538.

[26] A. W. Baggett, F. Guo, B. Li, S. Liu, F. Jäkle, *Angew. Chem. Int. Ed.* **2015**, *54*, 11191.

[27] X. Liu, L. He, C. Wang, I. Hanif, H. Huang, W. Bu, *J. Mater. Chem. C* **2017**, *5*, 3156.

[28] J. J. Intemann, E. S. Hellerich, M. D. Ewan, B. C. Tlach, E. D. Speetzen, R. Shinar, J. Shinar, M. Jeffries-EL, *J. Mater. Chem. C* **2017**, *5*, 12839.

[29] Y. Hong, J. W. Y. Lam, B. Z. Tang, *Chem. Soc. Rev.* **2011**, *40*, 5361.

[30] J. Mei, Y. Hong, J. W. Y. Lam, A. Qin, Y. Tang, B. Z. Tang, *Adv. Mater.* **2014**, *26*, 5429.

[31] R. Hu, N. L. C. Leung, B. Z. Tang, *Chem. Soc. Rev.* **2014**, *43*, 4494.

[32] J. Mei, N. L. C. Leung, R. T. K. Kwok, J. W. Y. Lam, B. Z. Tang, *Chem. Rev.* **2015**, *115*, 11718.

[33] R. Yoshii, A. Hirose, K. Tanaka, Y. Chujo, *Chem. Eur. J.* **2014**, *20*, 8320.

[34] R. Yoshii, A. Hirose, K. Tanaka, Y. Chujo, *J. Am. Chem. Soc.* **2014**, *136*, 18131.

[35] S. Ito, A. Hirose, M. Yamaguchi, K. Tanaka, Y. Chujo, *Polymers* **2017**, *9*, 68.

[36] M. Yamaguchi, S. Ito, A. Hirose, K. Tanaka, Y. Chujo, *Polym. Chem.* **2018**, *9*, 1942.

[37] M. Yamaguchi, S. Ito, A. Hirose, K. Tanaka, Y. Chujo, *J. Mater. Chem. C* **2016**, *4*, 5314.

[38] R. D. McCullough, *Adv. Mater.* **1998**, *10*, 93.

[39] I. Osaka, R. D. McCullough, *Acc. Chem. Res.* **2008**, *41*, 1202.

[40] S. Ito, A. Hirose, M. Yamaguchi, K. Tanaka, Y. Chujo, *J. Mater. Chem. C* **2016**, *4*, 5564.

[41] M. Yamaguchi, S. Ito, A. Hirose, K. Tanaka, Y. Chujo, *Mater. Chem. Front.* **2017**, *1*, 1573.

[42] S. Ito, K. Tanaka, Y. Chujo, *Inorganics* **2019**, *7*, 100.

[43] S. Ito, M. Yaegashi, K. Tanaka, Y. Chujo, *Chem. Eur. J.* **2021**, *27*, 9302.

[44] C. Sinturel, M. Vayer, M. Morris, M. A. Hillmyer, *Macromolecules* **2013**, *46*, 5399.

[45] T.-Q. Nguyen, I. B. Martini, J. Liu, B. J. Schwartz, *J. Phys. Chem. B* **2000**, *104*, 237.

[46] J. Kim, T. M. Swager, *Nature* **2001**, *411*, 1030.

[47] E. Hennebicq, G. Pourtois, G. D. Scholes, L. M. Herz, D. M. Russell, C. Silva, S. Setayesh, A. C. Grimsdale, K. Müllen, J.-L. Brédas, D. Beljonne, *J. Am. Chem. Soc.* **2005**, *127*, 4744.

[48] I. A. Howard, J. M. Hodgkiss, X. Zhang, K. R. Kirov, H. A. Bronstein, C. K. Williams, R. H. Friend, S. Westenhoff, N. C. Greenham, *J. Am. Chem. Soc.* **2010**, *132*, 328.

[49] Y. Guo, Y. Jin, Z. Su, *Polym. Chem.* **2012**, *3*, 861.

[50] Y. Guo, Y. Jin, Z. Su, *Soft Matter.* **2012**, *8*, 2907.

[51] C. Fu, K. Jeng, Y. Li, Y. Hsu, M. Chi, W. Jian, J. Chen, *Macromol. Chem. Phys.* **2015**, *216*, 59.

[52] M. Beiner, H. Huth, *Nat. Mater.* **2003**, *2*, 595.

[53] S. Pankaj, M. Beiner, *J. Phys. Chem. B* **2010**, *114*, 15459.

[54] M. J. Frisch, G. W. Trucks, H. B. Schlegel, G. E. Scuseria, M. A. Robb, J. R. Cheeseman, G. Scalmani, V. Barone, G. A. Petersson, H. Nakatsuji, X. Li, M. Caricato, A. V. Marenich, J. Bloino, B. G. Janesko, R. Gomperts, B. Mennucci, H. P. Hratchian, J. V. Ortiz, A. F. Izmaylov, J. L. Sonnenberg, D. Williams-Young, F. Ding, F. Lipparini, F. Egidi, J. Goings, B. Peng, A. Petrone, T. Henderson, D. Ranasinghe, V. G. Zakrzewski, J. Gao, N. Rega, G. Zheng, W. Liang, M. Hada, M. Ehara, K. Toyota, R. Fukuda, J. Hasegawa, M. Ishida, T. Nakajima, Y. Honda, O. Kitao, H. Nakai, T. Vreven, K. Throssell, J. A. Montgomery, Jr., J. E. Peralta, F. Ogliaro, M. J. Bearpark, J. J. Heyd, E. N. Brothers, K. N. Kudin, V. N. Staroverov, T. A. Keith, R. Kobayashi, J. Normand, K. Raghavachari, A. P. Rendell, J. C. Burant, S. S. Iyengar, J. Tomasi, M. Cossi, J. M. Millam, M. Klene, C. Adamo, R. Cammi, J. W. Ochterski, R. L. Martin, K. Morokuma, O. Farkas, J. B. Foresman, and D. J. Fox, *Gaussian 16 Rev. C.01*, Wallingford, CT, **2016**.